How to derive the multi-fluid delta-SPH model

I. Hammani, G. Oger, D. Le Touzé
Ecole Centrale Nantes,
LHEEA Res. Dept. (ECN and CNRS), France
imadeddine.hammani@ec-nantes.fr

A. Colagrossi, S. Marrone
CNR-INSEAN
Marine Technology Research Institute
00128 Rome, Italy
andrea.colagrossi@cnr.it

***Abstract*—The present work is dedicated to a weakly-compressible multi-fluid SPH model where a diffusive operator is used in the Volumetric Strain Rate equation in order to remove instabilities from the pressure field. The present model is obtained through a combination of other exiting models [1]–[6]. The new proposed scheme is validated through numerous well-known benchmarks showing that we are able to recover the results already present in the literature but improving the solution of the pressure field.**

I. Introduction

The problem of simulating multi-phase flows has been the subject of many researches in the recent years due to the growing industrial demands, namely in the naval and aeronautical sectors. However, due to multiple physical and numerical constraints, the derivation of robust models is not straightforward. This is even more the case in the SPH context, as it is relatively a new numerical method compared to other theoretically well-established methods (FEM, VOF, etc.).

In 2003, Colagrossi and Landrini [1] derived the first SPH multi-fluid model able to treat density discontinuities in the fluid domain. In order to remove nonphysical high-frequencies of the pressure field, they used a periodic density filtering which, however, introduced numerical instabilities close to the free-surface for long time simulations (i.e. large number of time iterations). Español and Revenga [2] presented an SPH-DPD scheme where the particle volumes are evaluated through kernel summation; these volumes were called *thermodynamic volumes*, being non-coincident with the geometric ones. This approach was used by Hu and Adams [3] in 2006 for another multi-fluid SPH model. Conversely to [1], in the latter the density field is directly evaluated through the ratio between the particle masses and their thermodynamic volumes without the use of a continuity equation integrated in time. However, this SPH model cannot be used if a free-surface is present since the thermodynamic volumes cannot be evaluated in its proximity because of the kernel truncation. To circumvent this issue, in 2009 Grenier et al. [4] [5] proposed a multiphase model for interfacial and free-surface flows. They use a Volumetric Strain Rate equation for the time evolution of the thermodynamic volumes, while the density field is evaluated by a Shepard correction. The use of the Shepard kernel for the density field is, however, not sufficient to eliminate the instability of the pressure field at high wave numbers. In order to improve this SPH model in the present work we propose the use of the diffusive term introduced in the δ-SPH scheme by [6]. Since in [4] the continuity equation is expressed for the thermodynamic volumes, the diffusive term has to be modeled in a different way with respect to [6].

Therefore, the present paper is structured as follows. First, the thought process behind the derivation of the model is presented. Then, results of several test cases in both single-phase and multi-phase configurations will be showcased, highlighting the capabilities of the model in simulating interfacial flows, with or without the presence of a free-surface.

II. Description of the proposed multi-fluid δ-SPH model

In the following two ways of derivation of the multi-fluid-δ-SPH model are presented. The first one is using the model developed by Español and Revenga [2]. The second one comes from the works of [1] and [4]. We show that the two formulations provide equations which are very similar and give results quite close each other.

A. Derivation using evaluation of particles volumes by direct kernel summation

In Español and Revenga (2003) [2] the DPD-SPH models are derived estimating the volume V_i of a generic i^{th} particle as:

$$V_i = \frac{1}{\sum_j W_{ij}} \tag{1}$$

It is important to note that V_i is not the geometric volume of particle i, the sum $\sum_j V_j$ does not coincide with the total volume of the domain V_T. However, if a large number of particles is used, the equality between $\sum_j V_j$ and geometric volume V_T is expected to be verified since the kernel function W is normalized to unity.

Because of the difference between V_i and the the geometric volume occupied by the particle i, in Español and Revenga (2003) V_i are name "thermodynamic volumes". It follows, that in all the SPH models the particles volumes are "thermodynamic" and not geometrical volumes.

Based on this approximation, the density of particle i is defined as:

$$\rho_i = m_i \sum_j W_{ij} \tag{2}$$

This approximation handles density discontinuities by preventing neighbouring particles masses from contributing

to the evaluation of the particle densities, especially in the presence of other phases around.

Next, we need to derive the momentum equation. We write the Lagrangian $\mathcal{L}$ of a generic particles system as:

$$\mathcal{L} = \sum_j m_j \frac{\boldsymbol{u}_j^2}{2} - m_j U(t, x_j) - m_j e(\rho_j, s_j) \tag{3}$$

where U is a generic energy potential per unit of mass, and e is the internal energy related to the particle-particle interaction, supposed to be a function of the density and entropy fields. The dynamics of the system is described by:

$$\frac{d}{dt}\left(\frac{\partial \mathcal{L}}{\partial \boldsymbol{u}_i}\right) - \frac{\partial \mathcal{L}}{\partial \boldsymbol{r}_i} = 0 \tag{4}$$

where dissipative and boundary forces are not taken into consideration. Further details on these aspects are presented in Colagrossi et al. [7]. The system of ordinary differential equations needs to be closed. Following the first law of thermodynamics, the pressure p_i is obtained through the variations of the specific internal energy as a consequence of the variations of the density field :

$$p_i = \rho_i^2 \left.\frac{\partial e_i}{\partial \rho_i}\right|_s \tag{5}$$

In the scope of the present work, we suppose that the entropy is constant since we are not concerned with the irreversible thermodynamic exchanges between particles. Therefore, substituting (3) in (4) and using (5) we get:

$$m_i \frac{d\boldsymbol{u}_i}{dt} - m_i \boldsymbol{f}_i + \sum_j m_j \frac{p_j}{\rho_j^2} \frac{\partial \rho_j}{\partial \boldsymbol{r}_i} = 0 \tag{6}$$

where $\boldsymbol{f}_i = -\partial U / \partial \boldsymbol{r}_i$ is a generic force field, such as gravity. Then, using (2) we get our momentum equation:

$$m_i \frac{d\boldsymbol{u}_i}{dt} = -\sum_j (p_i V_i^2 + p_j V_j^2) \nabla_i W_{ij} + m_i \boldsymbol{f}_i \tag{7}$$

When a free-surface is present in the fluid domain the equation (1) yields wrong volumes near the free-surface due to the truncation of the kernel support, which in turn results in erroneous densities and pressures.

Thus, in the present context of multi-fluids with free-surfaces, we circumvent this free-surface issue by writing the time derivative of (1) as follows:

$$V_i \sum_j W_{ij} = 1 \Rightarrow \frac{dV_i}{dt} \sum_j W_{ij} + V_i \frac{d \sum_j W_{ij}}{dt} = 0$$
$$\Rightarrow \frac{dV_i}{dt} \frac{1}{V_i} = -V_i \sum_j \frac{dW_{ij}}{dt}$$

which yields the following expression:

$$\frac{dV_i}{dt} = V_i^2 \sum_j (\boldsymbol{u}_j - \boldsymbol{u}_i) \cdot \nabla W_{ij} \tag{8}$$

It important to underline that the use of (8) implies a choice on the initial conditions. Usually at $t = 0$ the particles are positioned in a regular way on the domain (see emphe.g. [8]) and therefore, at least for this initial instant, the particle volumes can be initialize with the geometrical volumes. This is not case when equation (1) is used.

Once the particles volumes are evaluated through the time integration of (8), the density field needs to be evaluated. Again in presence of a free-surface also equation (2) cannot be used, and following [1] the simple relation:

$$\rho_i(t) = \frac{m_i}{V_i(t)} \qquad m_i = \rho_i(t=0) V_i(t=0) \tag{9}$$

is used, where the particles masses are set by the initial conditions and remain constant during the time evolution. A different choice is made in the Grenier et al. [4] model, as explained in the next subsection II-B.

Once the density field is evaluated the pressure is obtained through the use of a stiff equation of state:

$$p_i = \frac{\rho_{0\chi} c_{0\chi}^2}{\gamma_\chi} \left[\left(\frac{\rho_i}{\rho_{0\chi}} \right)^{\gamma_\chi} - 1 \right] + p_b \tag{10}$$

where γ_χ is the polytropic coefficient of phase χ, and p_b is a background pressure constant in all the fluid domain.

B. Derivation using the Volumetric Strain Rate equation

Differently from Espanol and Revenga [2], in [4] and [5] the Volumetric Strain Rate equation is directly used to evaluate the particles volumes:

$$\frac{dV}{dt} = V \,\mathrm{Div}(\boldsymbol{u}) \quad \Rightarrow \quad \frac{dV_i}{dt} = V_i \sum_j (\boldsymbol{u}_j - \boldsymbol{u}_i) \cdot \nabla W_{ij} \, V_j \tag{11}$$

In this equation the velocity divergence is approximated within the SPH framework as in [1]:

$$\langle \mathrm{Div}(\boldsymbol{u}) \rangle_i = \sum_j (\boldsymbol{u}_j - \boldsymbol{u}_i) \cdot \nabla W_{ij} \, V_j \tag{12}$$

This SPH model differs from other SPH models where a continuity equation for the density field is used. Similarly to Espanol and Revenga [2] the particles volumes are derived and density is successively evaluated. In reality in the Grenier et al. model the velocity divergence relied on a normalizing integral Γ which is not used here, since it was found to have negligible effect on the results. Beside this, eq. (11) is quite similar to the equation (8), the only difference being a volume V_j which is replaced by a volume V_i. This change, however, has a limited effect since in the present model the particles have always similar volumes (while densities and masses can be quite different in the multi-fluid context).

Once the particle volumes are evaluated by the time integration of (11), in the Grenier et al. model [4] a Shepard interpolation of the particles masses is used for evaluating the density field:

$$\begin{cases} \rho_i = \sum_j m_j \, W_{ij}^S, \qquad W_{ij}^S := \dfrac{W_{ij}}{\sum_k W_{ik} V_k} \\ m_i = \rho_i(t=0) V_i(t=0) \end{cases} \tag{13}$$

Again the particles masses are evaluated by the initial conditions and then they remain fixed in time (ensuring intrinsically the mass conservation). Note that the Shepard kernel W^S requires the knowledge of the particles volumes V_k. As reported in [4], it is important to underline that since the definition (13) is used, the direct link $m_i = \rho_i V_i$ is not strictly verified in this model. As described above, once the density is evaluated, the pressure is given in the different fluid phases by the equation of state (II-A).

Using the divergence operator (12) the corresponding pressure gradient derived through energy considerations (see [9]) is:

$$\langle \nabla p \rangle_i = \sum_j (p_j + p_i) \nabla W_{ij} V_j \tag{14}$$

which differs from the one in (II-A); the latter can be rewritten as:

$$\langle \nabla p \rangle_i = \sum_j \left(\frac{V_j^2 p_j + V_i^2 p_i}{V_i V_j} \right) \nabla W_{ij} V_j \tag{15}$$

Again the two equations are not so different considering the regular and almost homogeneous particle volume distributions adopted in these SPH models.

Similarly to what already discussed above, thanks to the use of equations (11) and (15), also this model is able to simulate interfacial flows in the presence of a free-surface.

Regarding the Grenier et al. model, this model was also limited to low Reynolds number simulations, otherwise the pressure fields became irregular as the Monaghan/Morris viscous operators fail to properly stabilize the scheme. Even in the single-phase simulations when the viscosity level is reduced the Grenier et al. model did not yield satisfactory results.

For this reason we want to extend the δ-SPH diffusive terms of Antuono et al. [6] in our multi-phase context, resulting in pressure fields with no high-frequency oscillations.

C. The multi-fluid δ-SPH model

For a reminder the δ-SPH scheme reads:

$$\begin{cases} \dfrac{d\rho_i}{dt} = -\rho_i \displaystyle\sum_j (\boldsymbol{u}_j - \boldsymbol{u}_i) \cdot \nabla W_{ij} V_j + \delta h c_0 \sum_j \boldsymbol{\psi}_{ji} \cdot \nabla W_{ij} V_j \\ \rho_i \dfrac{d\boldsymbol{u}_i}{dt} = -\displaystyle\sum_j (p_j + p_i) \nabla W_{ij} V_j + \rho_i \boldsymbol{f}_i + \alpha h c_0 \rho_0 \sum_j \pi_{ij} \nabla W_{ij} V_j \\ \dfrac{d\boldsymbol{r}_i}{dt} = \boldsymbol{u}_i; \quad p_i = p_i(\rho_i, \rho_0, c_0, \gamma) \end{cases} \tag{16}$$

where

$$\begin{cases} \boldsymbol{\psi}_{ji} = 2(\rho_j - \rho_i) \dfrac{\boldsymbol{r}_{ji}}{|\boldsymbol{r}_{ij}|^2} - (\nabla^L \rho_i + \nabla^L \rho_j) \\ \pi_{ij} = \dfrac{\boldsymbol{u}_{ij} \cdot \boldsymbol{r}_{ij}}{|\boldsymbol{r}_{ij}|^2} \end{cases} \tag{17}$$

and $\nabla^L \rho_i$ is the renormalized density gradient [10] defined as:

$$\begin{aligned} \nabla^L \rho_i &= \sum_j (\rho_j - \rho_i) \mathbb{L}_i \nabla W_{ij} V_j \\ \mathbb{L}_i &= \left[\sum_j (\boldsymbol{r}_j - \boldsymbol{r}_i) \otimes \nabla W_{ij} V_j \right]^{-1} \end{aligned} \tag{18}$$

The main problem to extend the δ-SPH scheme's to the multi-fluid SPH framework is that the continuity equation has be replaced by the Volumetric Strain Rate equation making the adaptation of the diffusion terms not trivial.

An "intuitive" way to adapt the $\boldsymbol{\psi}_{ji}$ term is to simply rewrite it in terms of particles volumes:

$$\boldsymbol{\psi}_{ji} = 2(V_j - V_i) \frac{\boldsymbol{r}_{ji}}{|\boldsymbol{r}_{ji}|^2} \tag{19}$$

The equivalent terms related to $\nabla^L \rho$ are not more necessary since the density has a linear hydrostatic component while this is not the case when looking the volumes spatial distribution (conversely to the particles masses). However, this method proved unsuccessful in practice and the reason is yet to be understood.

Instead, we rewrite $\boldsymbol{\psi}_{ji}$ term as follows:

$$\boldsymbol{\psi}_{ji} = V_i \left[\left(\frac{\rho_j}{\rho_i} - 1 \right) \frac{\boldsymbol{r}_{ji}}{|\boldsymbol{r}_{ji}|^2} - \frac{1}{\rho_i} \left(\nabla^L \rho_i + \nabla^L \rho_j \right) \right] \tag{20}$$

To sum up, the complete ODEs for the particles system of the proposed model, written for a generic ith particle of phase χ, are:

$$\begin{cases} \dfrac{dV_i}{dt} &= V_i \displaystyle\sum_j (\boldsymbol{u}_j - \boldsymbol{u}_i) \cdot \nabla W_{ij} V_j - \delta h c_{0\chi} \sum_{j \in \chi} \boldsymbol{\psi}_{ji} \cdot \nabla W_{ij} V_j \\ \rho_i &= \displaystyle\sum_j m_j W_{ij}^S \\ p_i &= \dfrac{\rho_{0\chi} c_{0\chi}^2}{\gamma_\chi} \left[\left(\dfrac{\rho_i}{\rho_{0\chi}} \right)^{\gamma_\chi} - 1 \right] \\ \rho_i \dfrac{d\boldsymbol{u}_i}{dt} &= -\displaystyle\sum_j (p_i + p_j) \nabla W_{ij} V_j + \rho \boldsymbol{f}_i + \\ &\quad + \alpha h c_{0\chi} \rho_{0,i} \displaystyle\sum_{j \in \chi} \pi_{ij} \nabla W_{ij} V_j \\ \dfrac{d\boldsymbol{r}_i}{dt} &= \boldsymbol{u}_i \end{cases} \tag{21}$$

The parameter δ is set equal to 0.1 for all the simulations. Note that the sums of the diffusive terms for both the Volumetric Strain Rate equation and momentum equation are made only over particles of the same phase as particle i. This is motivated by the fact that we do not want to alter the explicit treatment of the density discontinuities by allowing a diffusion mechanism across the interface between the phases.

III. Validation

The proposed model was validated through 3 classic test cases: a hydrostatic problem, an oscillating ellipse and a dam-break. These simulations have the advantages of being easy to implement and with well-known experimental data and/or

analytical solutions. In order to highlight the capabilities of the model, each simulation was run in single-phase and multi-phase configurations. In order to impose the weakly-compressibility of the model, the artificial sound speed c_0 is chosen to satisfy the following:

$$c_0 \geq 10 \max\left(U_{\max}, \sqrt{\frac{p_{\max}}{\rho_0}}\right) \tag{22}$$

where $U_{\max}$ and $p_{\max}$ are the maximum expected pressure and velocity. In multi-phase cases, the artificial sound speed of the lighter phase c_l was chosen according to the Colagrossi et al. [1] formula:

$$c_l = c_h \sqrt{\gamma_l \rho_{0h}/(\gamma_h \rho_{0l})} \tag{23}$$

where c_h is the artificial sound speed of the heavier phase, computed via (22). Finally, the time steps are computed as follows:

$$\Delta t = \text{CFL}\frac{2h}{c_{\max}} \tag{24}$$

where h is the smoothing length. Using a 4th order Runge-Kutta scheme for time integration the CFL number can be set equal to 0.75.

A. *Long-time evolution for the hydrostatic test-case*

For the single-phase hydrostatic problem, a two-dimensional tank is half-filled with water at rest. For the air-water simulation, the other half is filled with air. Here, the background pressure was set to $p_b = 0.1 p_{max}$, otherwise we observe a nonphysical void at the interface between the phases as shown in Figure (1), due to the occurrence of negative pressures in the interface zone.

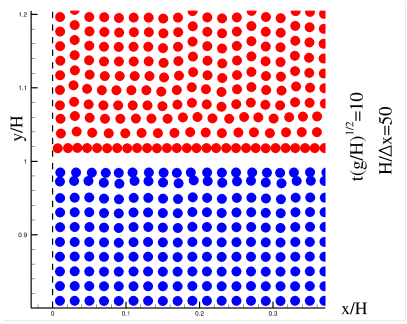

Fig. 1: Example of the nonphysical void between air (red) and water (blue).

The long-time evolution of the hydrostatic cases was monitored up to 300 seconds. Figure (2) shows the initial and final pressure profiles. The correct hydrostatic solution is retrieved for both single-phase and multi-phase configurations. The particles generally stay on the initial Cartesian grid, although a small perturbation of particles is observed just underneath the free-surface. Figure (3) shows the kinetic energy evolution. It rapidly decreases towards zero, showing good stability of the model. The kinetic energy of the air-water simulation is two-order of magnitude less than its

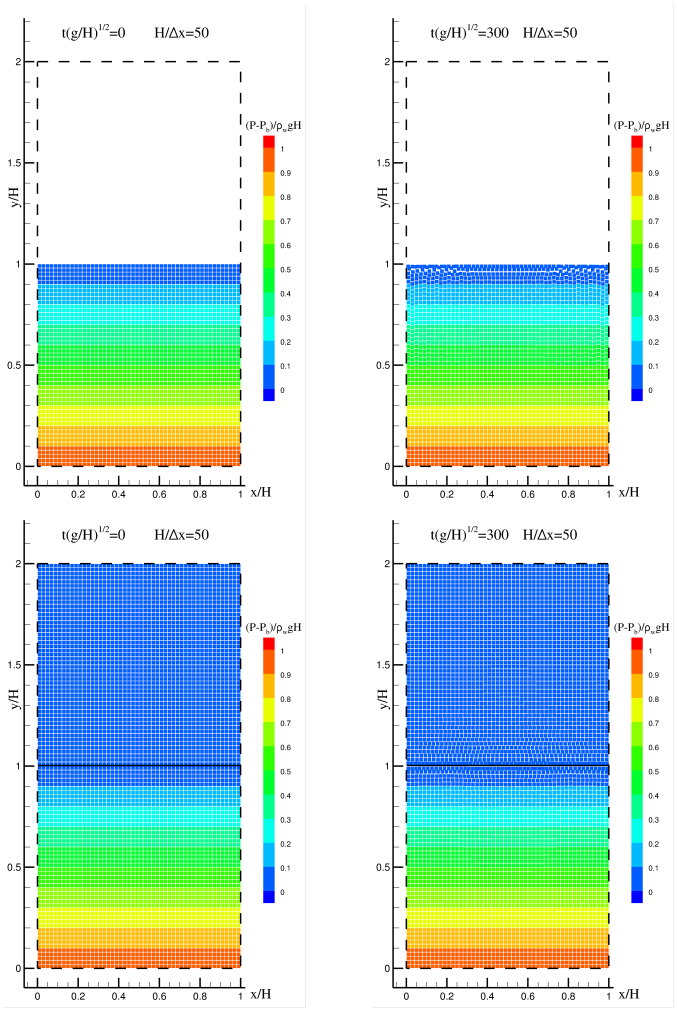

Fig. 2: Initial and final instants of the hydrostatic simulations. The black solid line denotes the interface between air and water.

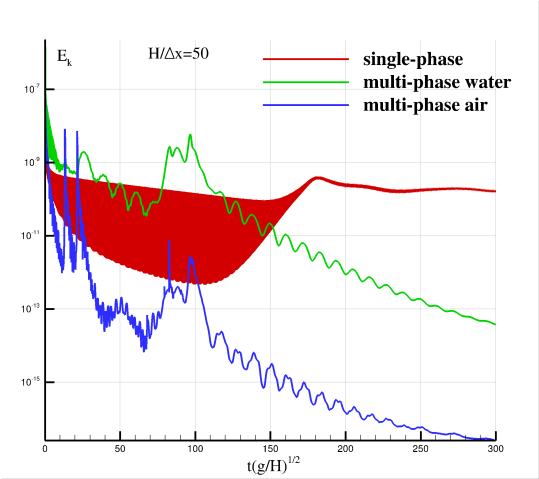

Fig. 3: Evolution of the kinetic energy for the water-only and air-water hydrostatic cases.

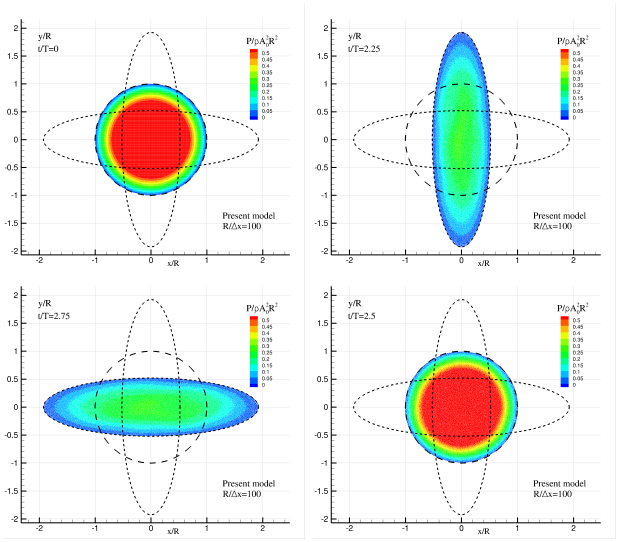

Fig. 4: Evolution of the a single-phase oscillating drop at different times (displayed in clockwise order). The the dashed lines represent the analytical solution analytical solution.

single-phase counterpart. This is due to the addition of a background pressure in the multi-phase case, which induces more numerical diffusion.

B. Oscillating drop: single and two-phases

1) Single-phase case: We consider a 2D fluid bubble evolving in a quadratic potential $1/2\Omega^2(x^2+y^2)$. The fluid is inviscid ($\alpha = 0$), and the radius of the disk is R. The velocity field is assumed to have the following form:

$$\begin{aligned} u &= A(t)x \\ v &= -A(t)y \end{aligned} \tag{25}$$

and we set $A(0) = \Omega$. Following the study of Monaghan and Rafiee [11], under these conditions the drop should evolve periodically as an oscillating ellipse. Figure (4) presents the initial and deformed shapes of the fluid bubble. The free-surface evolution of the ellipses in comparison with the analytical solution is satisfactory. This is further illustrated in Figure (5), where the predicted evolution of the ellipse semi-axis $a(t)$ is in very good agreement with its analytical counterpart.

A convergence study was made in order to monitor the mechanical energy. Figure (6) plots the evolution of the normalized mechanical energy for 3 discretizations. Similarly to Antuono et al. [12], for increasing numbers of particles, smaller dissipations of the mechanical energy occur due to the presence of the diffusive term in the continuity equation.

2) Multi-phase case: This time we consider two initial concentric circular bubbles of fluids Inner and Outer. The heavier fluid occupies the inner circular region of radius $R/2$, while the lighter fluid occupies the region between the outer circle of radius R and the inner circle. Both fluids evolve in the quadratic potential $1/2\Omega^2(x^2+y^2)$, and we keep $A(0) = \Omega$.

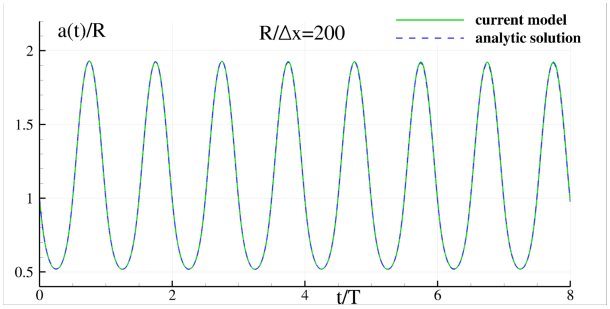

Fig. 5: Comparison between the predicted evolution of the semi-axis $a(t)$ and the analytical solution.

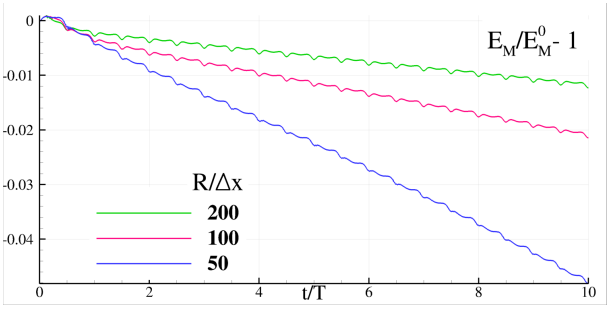

Fig. 6: Time history of the normalized mechanical energy variation for different discretizations.

Note that unlike [11], in the current simulation no damping technique was needed to initialize the pressure field. Figure (7) illustrates the initial configuration of the problem, with a density ratio $\rho_{inner}/\rho_{outer} = 100$. Figure (8) shows the evolution of the outer ellipse's semi-axis $a(t)$ for different density ratios. As predicted by the analytical solution, the motion of $a(t)$ is unaffected by the density ratio. The pressure

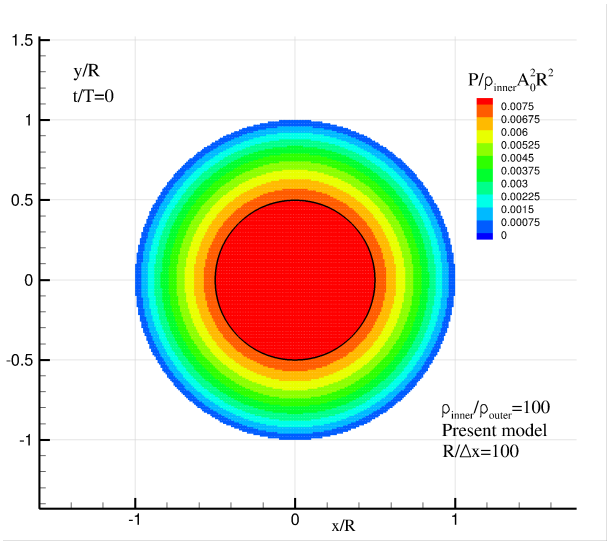

Fig. 7: Initial state of the concentric circular bubbles. The solid black line denotes the interface between the fluids.

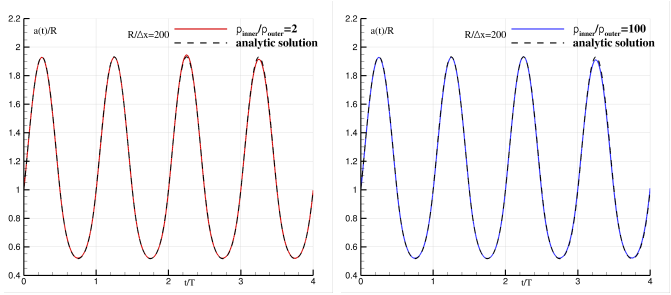

Fig. 8: Outer ellipse semi-axis evolution for a density ratio of 2 (left) and 100 (right) vs the incompressible solution. The axis evolution does not vary with the density ratio.

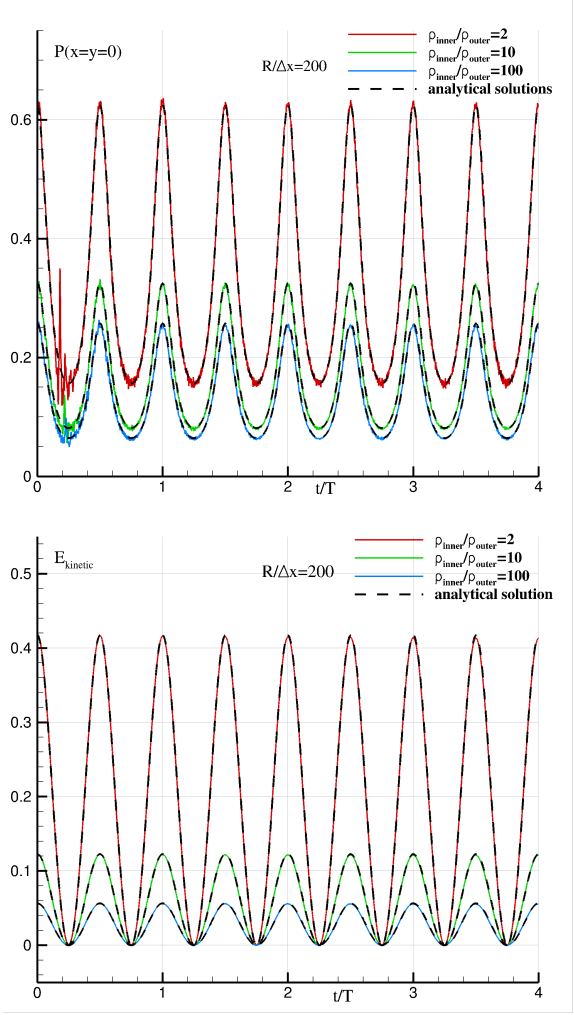

Fig. 9: Top:Pressure measured at the center of the inner bubble for different density ratios. Bottom: Evolution of the system's kinetic energy for different density ratios

at the center of the inner bubble is plotted in Figure (9). A small perturbation at the end of the first half-period occurs due to the compressibility of the model, but all in all, it is clear that the current model's computed pressure follows

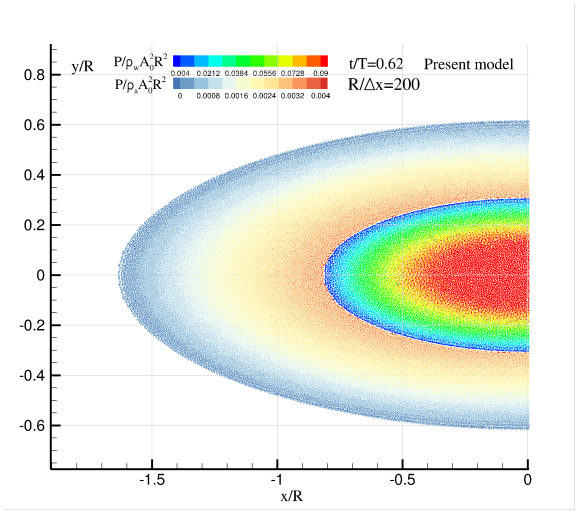

Fig. 10: Top: Pressure field in the inner and outer bubbles.

closely the incompressible solution. Overall, the model yields satisfactory pressure fields in both the inner and outer phases, as shown in Figure (10). The kinetic energies are plotted in bottom plot of Figure (9) for different density ratios. Once again, there is a very good agreement between the computed and incompressible solutions of the problem, showcasing the satisfactory accuracy of the proposed model.

C. Dam Break flow: single and two-phases

The third test case is a dam-break impacting a vertical wall as described in [1]. The initial problem is illustrated in Figure (11), where P_1 is a pressure probe. Snapshots of the dam-break flow evolution in the single-phase configuration are shown in Figure (12). The model clearly handles well the presence of the free-surface. Also, thanks to the addition of the diffusive terms in the present model, no spurious oscillations of pressure are observed. This is the main improvement upon [4] as also illustrated in Figure (13), which highlights the differences in the resulting pressure fields obtained with the proposed model and the Grenier et al. model. In particular it is possible to

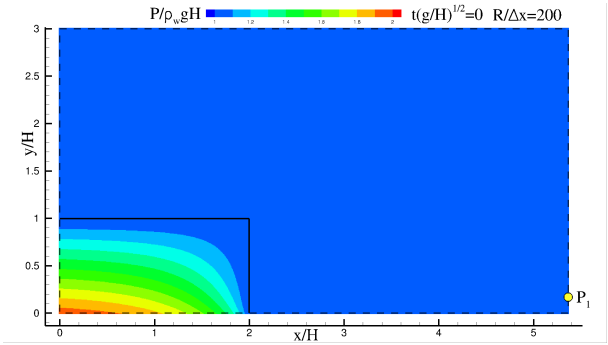

Fig. 11: Initial configuration of the multi-phase dam-break problem. The black solid line denotes the interface between the phases.

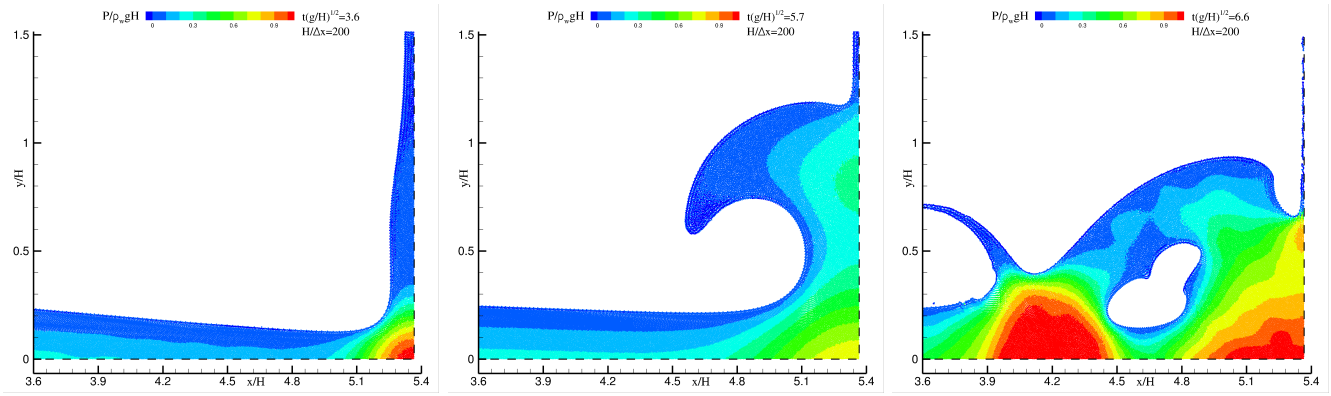

Fig. 12: Snapshots of the single-phase dam-break flow at different times.

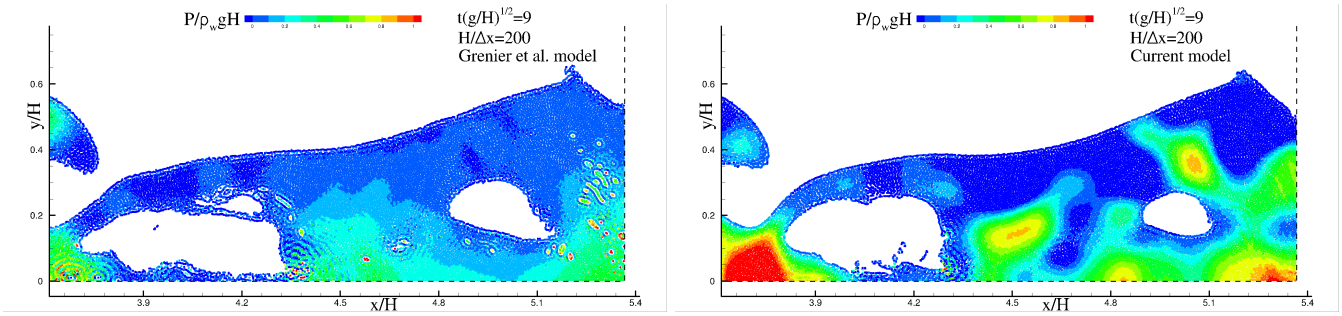

Fig. 13: Snapshot of the dam-break flow at $t(g/H)^{1/2} = 9$, using the Grenier et al. model (top) and the current model (bottom).

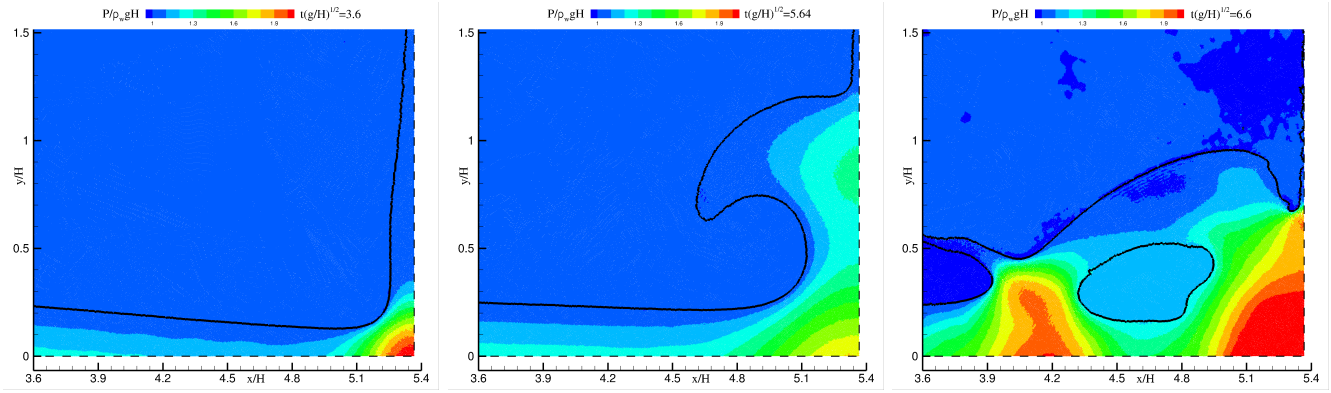

Fig. 14: Snapshots of the multi-phase dam-break flow at different times.

observe that the Grenier et al. model suffers from local isolated pressure discontinuity here which are formed during impacts and remain unaltered during the flow evolution.

Another simulation of the same dam-break flow was run, this time in a multi-phase configuration. The adopted density ratio is $\rho_{water}/\rho_{air} = 1000$. Figure (14) shows the dam-break evolution and the pressure field in the water phase. The latter is in very good agreement with its single-phase equivalent, as the pressure levels inside the water are almost identical in both cases up to the cavity closure, after which the air cushioning effects become relevant (see third plot of Figure 14) and the two flow evolutions do not behave anymore in the same manner. This is confirmed looking at the pressure measured at the probe P_1 as shown in Figure (15). Both models agree very well up to around $t(g/H)^{1/2} = 6.0$, which corresponds to the first cavity closure. Then the two-phase model predicts a pressure oscillation due to the entrapped air bubble which is not predicted by the single-phase simulation as this cavity is void. The latter collapses in a flat impact around $t(g/H)^{1/2} = 8.0$ producing a transfer of energy from mechanical energy to internal one, in the form of travelling acoustic waves which are visible in bottom plot of Figure 12 (see also [13] for a

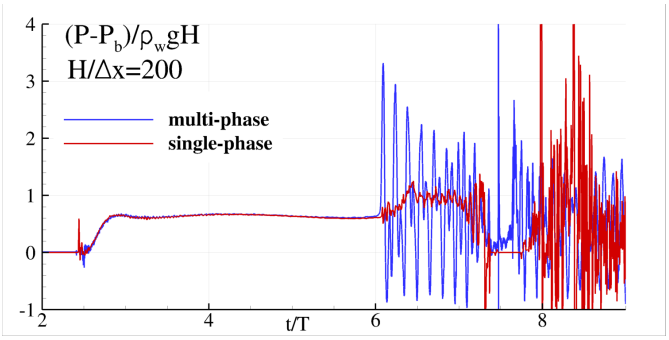

Fig. 15: Time history of the pressure at the probe P1.

detailed discussion about this phenomenon).

IV. Conclusion and Perspectives

A weakly-compressible SPH model was derived and successfully simulated single-phase and multi-phase flows in the presence of a free-surface. The accuracy and robustness of the model was highlighted through three test cases, and the comparison of its results with the analytical solutions present in the literature yielded satisfactory results. On top of its versatility, the proposed model has the advantage of computing pressure fields with no high-frequency oscillations thanks to the adaptation of the diffusive terms of Antuono et al.'s δ-SPH scheme [6]. This advantage would prove very useful for the simulation of multi-phase cases where accurate predictions of the pressure loads is crucial, such as ditching problems. In the future, this model can be improved by including surface tension and viscosity effects, by increasing its accuracy through the adaptation of a shifting technique and by extending its scope to three-dimensional flows.

Acknowledgements

The research leading to these results has received funding from the European Union's Horizon 2020 Research and Innovation Programme (Grant No. 724139). The SPH simulations performed under the present research have been obtained using the SPH-Flow solver, software developed within a collaborative consortium composed of Ecole Centrale de Nantes, Next Flow Software company and CNR-INSEAN.

References

[1] A. Colagrossi and M. Landrini, "Numerical simulation of interfacial flows by smoothed particle hydrodynamics," *J. Comput. Phys.*, vol. 191, no. 2, pp. 448–475, Nov. 2003.

[2] P. Español and M. Revenga, "Smoothed dissipative particle dynamics," *Phys. Rev. E*, vol. 67, p. 026705, Feb 2003.

[3] X. Hu and N. Adams, "A multi-phase sph method for macroscopic and mesoscopic flows," *Journal of Computational Physics*, vol. 213, no. 2, pp. 844–861, 2006.

[4] N. Grenier, M. Antuono, A. Colagrossi, D. L. Touzé, and B. Alessandrini, "An hamiltonian interface sph formulation for multi-fluid and free surface flows," *Journal of Computational Physics*, vol. 228, no. 22, pp. 8380–8393, 2009.

[5] N. Grenier, D. L. Touzé, A. Colagrossi, M. Antuono, and G. Colicchio, "Viscous bubbly flows simulation with an interface sph model," *Ocean Engineering*, vol. 69, pp. 88–102, 2013.

[6] M. Antuono, A. Colagrossi, and S. Marrone, "Numerical diffusive terms in weakly-compressible sph schemes," *Computer Physics Communications*, vol. 183, no. 12, pp. 2570–2580, 2012.

[7] A. Colagrossi, D. Durante, J. Bonet Avalos, and A. Souto-Iglesias, "Discussion of stokes' hypothesis through the smoothed particle hydrodynamics model," *Phys. Rev. E*, vol. 96, p. 023101, Aug 2017.

[8] A. Colagrossi, B. Bouscasse, M. Antuono, and S. Marrone, "Particle packing algorithm for SPH schemes," *Computer Physics Communications*, vol. 183, no. 2, pp. 1641–1683, 2012.

[9] A. Colagrossi, M. Antuono, and D. Le Touzé, "Theoretical considerations on the free-surface role in the Smoothed-particle-hydrodynamics model," *Physical Review E*, vol. 79, no. 5, p. 056701, 2009.

[10] M. Antuono, A. Colagrossi, S. Marrone, and D. Molteni, "Free-surface flows solved by means of sph schemes with numerical diffusive terms," *Computer Physics Communications*, vol. 181, no. 3, pp. 532–549, 2010.

[11] J. J. Monaghan and A. Rafiee, "A simple sph algorithm for multi-fluid flow with high density ratios," *International Journal for Numerical Methods in Fluids*, vol. 71, no. 5, pp. 537–561.

[12] M. Antuono, S. Marrone, A. Colagrossi, and B. Bouscasse, "Energy balance in the δ-sph scheme," *Computer Methods in Applied Mechanics and Engineering*, vol. 289, pp. 209–226, 2015.

[13] S. Marrone, A. Colagrossi, A. Di Mascio, and D. Le Touzé, "Analysis of free-surface flows through energy considerations: Single-phase versus two-phase modeling," *Phys. Rev. E*, vol. 93, p. 053113, May 2016.